Journal of Medicinal Chemistry

pubs.acs.org/jmc

Article

Selective *C9orf72* G-Quadruplex-Binding Small Molecules Ameliorate Pathological Signatures of ALS/FTD Models

Aifang Cheng,[○] Changdong Liu,[○] Wenkang Ye,[○] Duli Huang, Weiyi She, Xin Liu, Chun Po Fung, Naining Xu, Monica Ching Suen, Wei Ye, Herman Ho Yung Sung, Ian Duncan Williams, Guang Zhu,* and Pei-Yuan Qian*

Cite This: *J. Med. Chem.* 2022, 65, 12825−12837

Read Online

ACCESS | Metrics & More | Article Recommendations | Supporting Information

ABSTRACT: The G-quadruplex (G4) forming *C9orf72* GGGGCC (G4C2) expanded hexanucleotide repeat (EHR) is the predominant genetic cause of amyotrophic lateral sclerosis (ALS) and frontotemporal dementia (FTD). Developing selective G4-binding ligands is challenging due to the conformational polymorphism and similarity of G4 structures. We identified three first-in-class marine natural products, chrexanthomycin A (**cA**), chrexanthomycin B (**cB**), and chrexanthomycin C (**cC**), with remarkable bioactivities. Thereinto, **cA** shows the highest permeability and lowest cytotoxicity to live cells. NMR titration experiments and *in silico* analysis demonstrate that **cA**, **cB**, and **cC** selectively bind to DNA and RNA G4C2 G4s. Notably, **cA** and **cC** dramatically reduce G4C2 EHR-caused cell death, diminish G4C2 RNA foci in $(G4C2)_{29}$-expressing Neuro2a cells, and significantly eliminate ROS in HT22 cells. In $(G4C2)_{29}$-expressing *Drosophila*, **cA** and **cC** significantly rescue eye degeneration and improve locomotor deficits. Overall, our findings reveal that **cA** and **cC** are potential therapeutic agents deserving further clinical study.

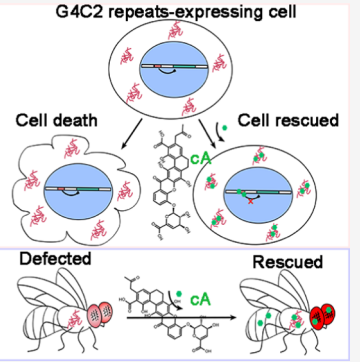

INTRODUCTION

Amyotrophic lateral sclerosis (ALS) is a devastating neurodegenerative disease characterized by motor neuron degeneration, neuromuscular weakness, and paralysis. It is regarded as one of the three incurable diseases by the World Health Organization. Approximately 50% of patients with ALS present cognitive impairments, and 13% develop concomitant frontotemporal dementia (FTD),[1] a progressive neurodegenerative disorder with neuron loss in frontal and temporal cortices. Although ALS and FTD severely threaten human health, over four decades of research have only yielded two drugs for ALS and none for FTD.[2] The two available ALS drugs are riluzole, a glutamate release inhibitor,[3] and edaravone, an antioxidant agent,[4] both with minimal efficacy and marginally prolonging survival.[5]

After identifying G4C2 expanded hexanucleotide repeat (EHR) in the first intron of the *C9orf72* gene as the most dominant genetic cause of ALS/FTD, insights from studying *C9orf72* ALS/FTD have inspired various therapeutic interventions for patients carrying this mutation.[6,7] Most healthy individuals carry less than 20 G4C2-repeats, but these expand up to thousands of repeats in ALS/FTD patients.[6] Nevertheless, the underlying mechanism of how G4C2 EHR contributes to ALS/FTD remains elusive. G4s, noncanonical secondary structures formed by *C9orf72* G4C2 DNA and RNA EHR,[8,9] have become attractive targets for developing ALS/FTD therapy.[10] In particular, small molecules targeting *C9orf72* G4C2 G4s seem especially advantageous, considering their pharmacological properties, such as the low molecular mass, which results in better blood−brain barrier (BBB) penetration. To date, several small molecules targeting G4s have been reported.[11−13] TMPyP4 is known to bind RNA $(G4C2)_8$ G4,[14,15] while other compounds bind G4C2 EHR hairpin structures;[16,17] although all of these compounds reduce RNA foci formation, whether or not they could block the translation of poly(GR) and poly(PR), the two most toxic dipeptide repeat (DPR) proteins contributing to neurodegeneration of ALS/FTD, remains unclear. In 2017, Simone et al. identified three structurally similar molecules (DB1246/DB1247/DB1273) that can bind and stabilize RNA G4C2 G4, decreasing RNA foci formation and levels of DPR proteins in neurons derived from patient iPSC and G4C2 EHR-expressing *Drosophila*.[18] However, in this study, we demonstrate that DB1246 nonselectively binds different types of G4s, possibly leading to strong side effects if applied to human subjects. TAT-BIND, a peptidyl nucleolar stress inhibitor, effectively inhibits RNA G4C2 EHR toxicities and significantly extends the life span of *Drosophila*. The proposed mechanism of action for this peptide in inhibiting EHR toxicity is through disrupting

Received: April 25, 2022
Published: September 15, 2022

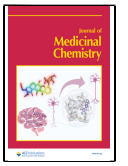

ACS Publications

© 2022 The Authors. Published by American Chemical Society

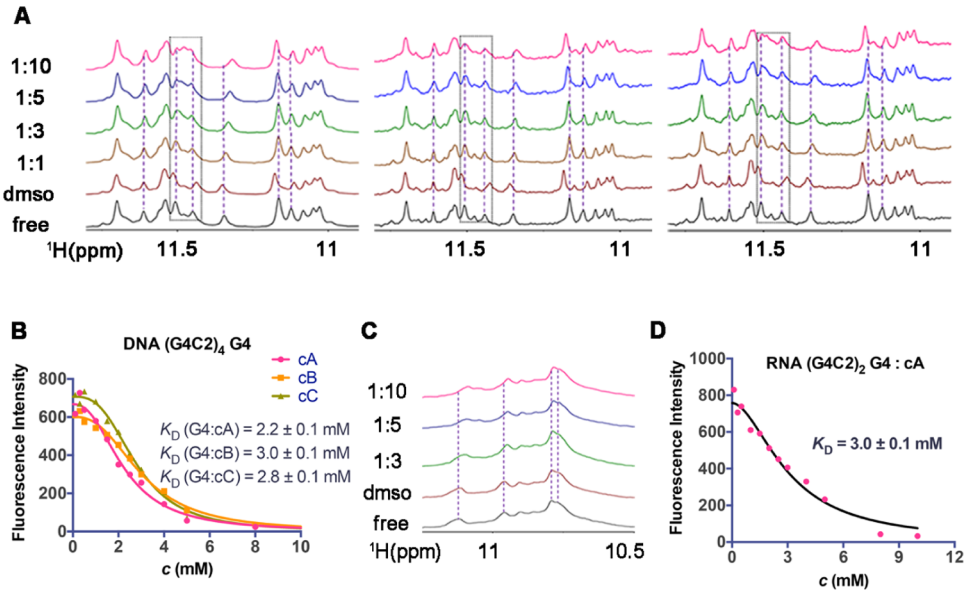

Figure 1. Compounds **cA**, **cB**, and **cC** bind DNA $(G4C2)_4$ G4 and RNA $(G4C2)_2$ G4. (A) Imino region of 1D ^{1}H NMR spectra of DNA $(G4C2)_4$ G4 and that titrated with compounds **cA** (left), **cB** (middle), and **cC** (right), respectively, at different ratios from 1:1 (light brown) to 1:10 (pink). (B) Fluorescence intensity assay of 3′- FAM-labeled DNA $(G4C2)_4$ G4 titrated with **cA**, **cB**, and **cC**, respectively, with concentration from 0.1 to 10 mM for determining the K_D value. The curve was fitted by nonlinear regression (One site — Specific binding with Hill slope). (C) Imino region of 1D ^{1}H NMR spectra of RNA $(G4C2)_2$ G4 and that titrated with compound **cA** at 1:3 (green), 1:5 (blue), and 1:10 (pink) ratios. (D) Fluorescence intensity assay of 3′- FAM-labeled RNA $(G4C2)_2$ G4 titrated with **cA** with concentration from 0.1 to 10 mM for determining the K_D value. The curve was fitted by nonlinear regression (One site — Specific binding with Hill slope).

the interaction between G4C2 RNA and nucleolin protein, restoring rRNA maturation, inhibiting mislocalization of nucleolin, and eventually suppressing nucleolar stress.[19] Unfortunately, peptide-based therapeutic approaches are limited due to proteolytic degradation and the short peptide half-lives. Other therapeutic strategies, such as oligonucleotide/RNA interference-based approaches and gene therapy, show promise in eliminating pathological RNA foci and repeat-containing *C9orf72* transcripts; however, these strategies require a better understanding of the function of the C9ORF72 protein because the reduction/loss of protein might affect wild-type gene expression and cell survival.[20−22] In brief, the existing treatments for *C9orf72* ALS/FTD show obvious disadvantages, including poor selectivity, questionable BBB permeability, short half-life, or biological safety problem. Therefore, safer and more effective treatments are desperately needed to be developed.

Better therapeutic agents should target disease mechanisms, which remain elusive due to the complex onset and progression (pathogenesis) of *C9orf72* ALS/FTD. Hypothetically, there are three underlying mechanisms of *C9orf72* ALS/FTD pathogenesis: (1) loss of *C9orf72* gene function, (2) toxic RNA foci formed by abnormal recruitment of RNA-binding proteins (RBPs) to RNA G4C2 EHR, and (3) toxic dipeptides from repeat-associated non-ATG (RAN) translation.[23,24] Therefore, targeting these toxicity factors that contribute to the disease pathogenesis is desirable to find superior therapeutic agents, and chemical compounds with improved pharmacological properties aiming at these interconnected risk factors would provide new perspectives on developing effective therapeutic agents.

Here, we identified three first-in-class marine-derived natural products, chrexanthomycin A (**cA**), chrexanthomycin B (**cB**), and chrexanthomycin C (**cC**), with novel chemical structures, significant neuroprotective activities, and high safety index. We demonstrated selective binding of these compounds to *C9orf72* DNA and RNA G4C2 G4s. When tested in Neuro2a cells, **cA** and **cC** dramatically reduced the $(G4C2)_{29}$-over-expression-induced cell death and diminished G4C2 RNA foci formation. We extended our biochemical and cellular tests to *C9orf72* ALS/FTD *Drosophila* models and demonstrated that **cA** and **cC** significantly rescued the eye degeneration phenotype of GMR-GAL4-$(G4C2)_{29}$ *Drosophila* and remarkably improved locomotor deficits of OK371-GAL4-$(G4C2)_{29}$ *Drosophila*. Furthermore, we performed *in silico* molecule docking analysis and found that the interaction between compounds and DNA $(G4C2)_4$ G4 was primarily driven by van der Waals forces and hydrogen bonds. Additionally, we illustrated that **cA** and **cC** showed ROS-scavenging ability in cells. Overall, our findings provide promising therapeutic agents that benefit *C9orf72* ALS/FTD patients by reducing G4C2-repeats-related toxicity.

RESULTS

Screening for *C9orf72* G4C2 G4s Binding Molecules from Marine Natural Products. Marine natural products provide a diverse database of model compounds for novel drug discovery due to their rich diversity, structure novelty, and high bioactivity.[25] G4s formed by *C9orf72* G4C2 EHR are deemed to be crucial in ALS/FTD pathogenesis and are regarded as therapeutic targets of *C9orf72* ALS/FTD. To discover novel compounds as drug candidates for treating ALS/FTD, we aim to screen selective G4C2 G4s binding molecules. We performed nuclear magnetic resonance (NMR) titration screening experiments on >1000 fermentation products from over 500 strains of marine bacteria and found that marine natural products, **cA**, **cB**, and **cC**, that were isolated from the fermentation product of *Streptomyces chrestomyceticus* showed significant binding to both DNA and RNA $(G4C2)_2$ G4s.

https://doi.org/10.1021/acs.jmedchem.2c00654
J. Med. Chem. 2022, 65, 12825−12837

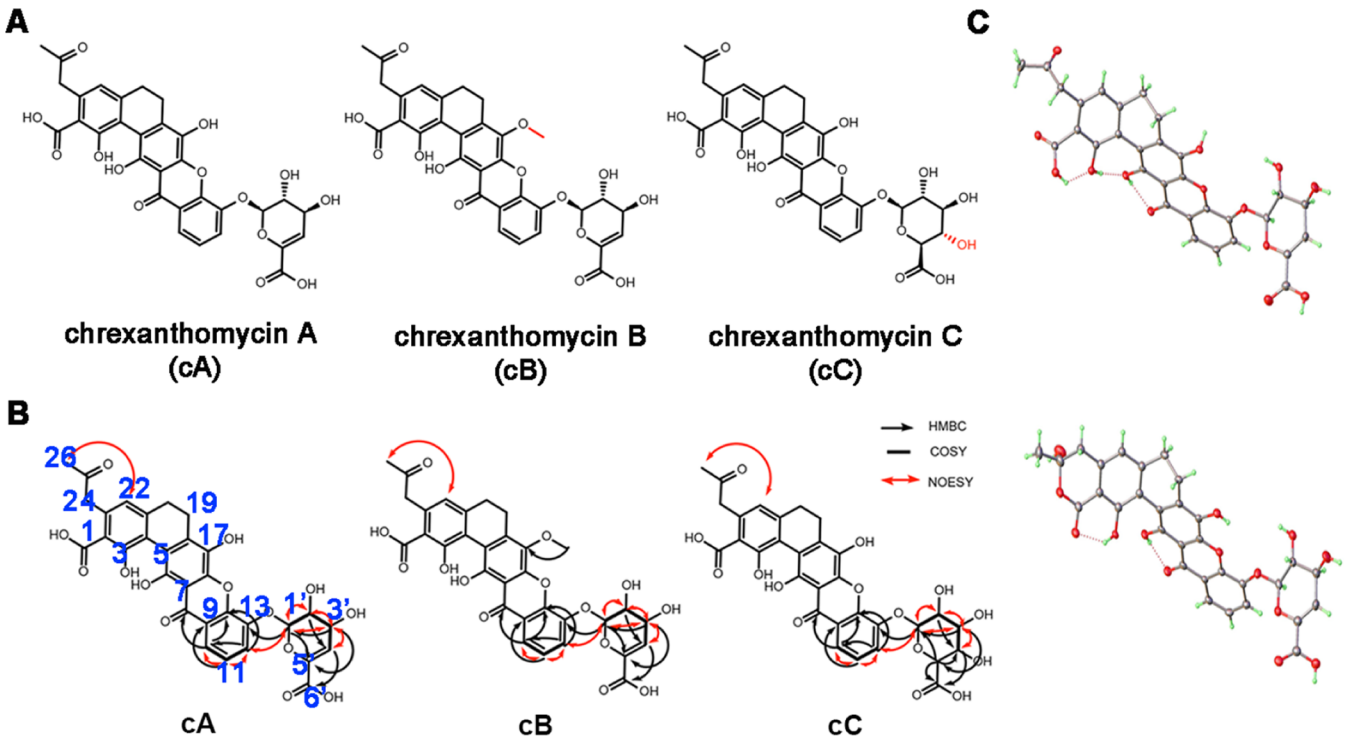

Figure 2. Compound structures. (A) Planar structures of compounds **cA**, **cB**, and **cC**. (B) Key HMBC, COSY, and NOESY correlations of compounds **cA**, **cB**, and **cC**. (C) Single-crystal X-ray diffraction confirms the NMR structure of **cA**—the open form (top) has exocyclic acetonyl and carboxylic acid groups; the cyclic form (bottom) has an α-hydroxylactone ring. Each form has 50% occupancy of molecular sites within the crystal.

Based on the one-dimensional (1D) ^{1}H NMR spectra of G4 titrated with different concentration ratios of **cA** (Figure 1A, left) from 1:1 to 1:10, apparent chemical shift changes in the peaks of G2/G10, G1/G14, G22, and G13 were observed, suggesting bindings between **cA** and DNA $(G4C2)_4$ G4. Similarly, **cB** and **cC** were predicted to have similar abilities to bind DNA $(G4C2)_4$ G4 (Figure 1A, middle and right). To measure the binding affinity, we performed a fluorescence intensity assay. The fluorescence intensity of 3′-FAM-labeled DNA $(G4C2)_4$ G4 was significantly decreased in a dose−response manner as the concentration of compounds (**cA**, **cB**, **cC**) increased. The binding affinity (K_D) of DNA $(G4C2)_4$ G4 with **cA**, **cB**, or **cC** were 2.2 ± 0.1, 3.0 ± 0.1, and 2.8 ± 0.1 mM, respectively (Figure 1B).

In addition to *C9orf72* EHR DNA, *C9orf72* EHR RNA also forms G4 structures, which might lead to the accumulation of abortive RNA transcripts and the loss of full-length RNA transcripts, disrupting normal translation.[8,26] The predicted RNA $(G4C2)_2$ G4 structure is a dimeric parallel form. A similar NMR titration experiment of RNA $(G4C2)_2$ G4 and **cA** was performed. Notable chemical shift changes were observed in 1D ^{1}H NMR spectra for RNA $(G4C2)_2$ G4 and **cA** at ratios of 1:3, 1:5, and 1:10 compared with the RNA $(G4C2)_2$ G4 only and dimethyl sulfoxide (DMSO) control spectra (Figure 1C). The binding affinity was measured by the fluorescence intensity assay using 3′-FAM-labeled RNA $(G4C2)_2$ G4 titrated with compound **cA** from 0.1 to 10 mM. The K_D was measured to be 3.0 ± 0.1 mM (Figure 1D).

To investigate whether the bindings between the G4C2 G4s and the compounds could be affected by potential parameters that existed in environmental or biological systems, such as pH or temperature, we recorded 1D ^{1}H NMR spectra of the G4C2 G4s in complex with the compounds at pH 6 and pH 7 in the temperature of 25, 35, and 45 °C, respectively (Figure S1). The NMR results clearly proved that the bindings of G4s with compounds were stable and could not be affected by the changes in pH or temperature (Figure S1). Furthermore, to validate the bindings, we also conducted circular dichroism (CD) spectra and melting curve recordings. As shown in Figure S2, we recorded the CD spectrum of *C9orf72* DNA and RNA G4C2 G4s in complex with the compounds at pH 6 and pH 7 at the temperature of 25 °C. The CD results showed that the interaction of G4s with the compounds does not change the conformation of G4s (Figure S2). The further CD melting experiments recorded on the complexes demonstrated that the compounds significantly changed the melting curve of RNA G4 at pH 7 (Figure S2), indicating the compounds increase the thermal stability of RNA G4. However, no significant changes were observed for DNA G4, possibly due to the high stability of DNA G4 composed of four G-tetrad layers (the melting temperature, T_m > 85 °C, or even higher).

Structure Elucidation of the Three *C9orf72* G4C2 G4s Binding Compounds. Structures of **cA**, **cB**, and **cC** (Figure 2A) were unambiguously elucidated through a combination of high-resolution mass spectrometry (HRMS), 1D (^{1}H, ^{13}C), and two-dimensional (2D) H−H correlation spectroscopy (COSY), heteronuclear single quantum coherence (HSQC), 1H detected heteronuclear multiple bond correlation (HMBC), nuclear Overhauser enhancement spectroscopy (NOESY) NMR spectra (Figures 2B and S3−S26) and X-ray crystallography (Figures 2C and S27−S28, Tables S1−S9), which confirmed the coexistence of open (Figure 2C, top) and cyclic (Figure 2C, bottom) forms of **cA**. This finding is helpful

https://doi.org/10.1021/acs.jmedchem.2c00654
J. Med. Chem. 2022, 65, 12825−12837

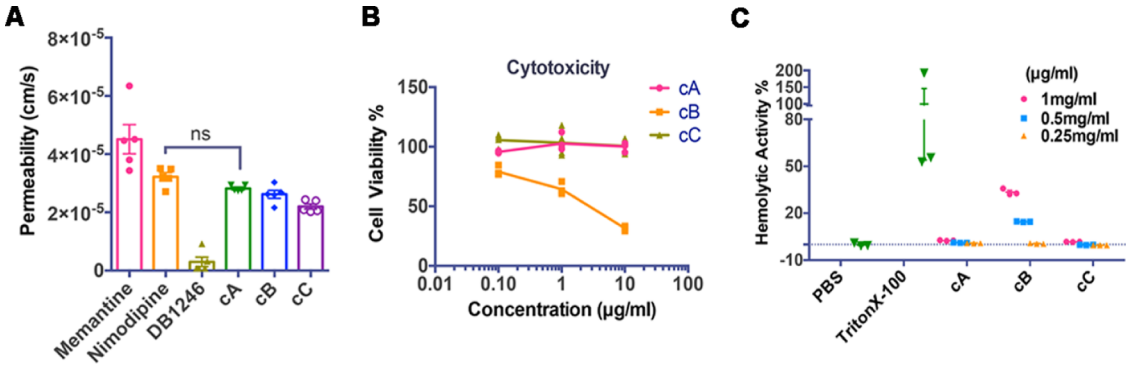

Figure 3. Safety evaluations of compounds. (A) Permeability (cm/s) of memantine, nimodipine, DB1246, **cA**, **cB**, and **cC**. n = 5 batches of cell cultures; p values were determined by one-way ANOVA (Tukey's multiple comparisons test). (B) Cytotoxicity of **cA**, **cB**, and **cC** was tested at concentrations of 0.1, 1, and 10 μg/mL (in molar units, **cA**: 0.16, 1.61, 16.13 μM; **cB**: 0.16, 1.58, 15.77 μM; **cC**: 0.16, 1.57, 15.67 μM) on HEK293T cells. n = 4 batches of cell cultures. (C) Hemolytic activity of **cA**, **cB**, and **cC** was tested at 0, 250, 500, and 1000 μg/mL (in molar units, **cA**: 0, 0.40, 0.81, 1.61 mM; **cB**: 0, 0.39, 0.79, 1.58 mM; **cC**: 0, 0.39, 0.78, 1.57 mM). Phosphate-buffered saline (PBS) and Triton X-100 served as negative and positive controls, respectively. n = 3 independent preparations. All data are mean ± s.e.m.

in understanding the mode of action of the interaction between **cA** and its target molecules.

Selectivity of cA on Binding *C9orf72* G4C2 G4s. G4s folded by the *C9orf72* EHR DNA and RNA show structural polymorphisms. Aside from four-repeat DNA G4C2 G4, two-repeat DNA G4C2 simultaneously form parallel and hybrid G4 conformations.[9,27] NMR titrations of different G4C2 sequences forming structures, including two-repeat DNA G4C2 G4, double-stranded DNA G4C2, single-stranded two-repeat DNA G4C2, double-stranded RNA G4C2, and four-repeat RNA G4C2 hairpin form with **cA** (Figure S29) were performed to test the binding selectivity. 1D ^{1}H NMR spectra showed that 1:10 titration of **cA** caused no chemical shift changes on the two-repeat DNA G4C2 G4 spectrum (Figure S29A). Similarly, 1:10 titration of **cA** had no effects on the spectra of double-stranded DNA G4C2 (Figure S29B), single-stranded two-repeat DNA G4C2 (Figure S29C), four-repeat RNA G4C2 hairpin form (Figure S29D), or double-stranded RNA G4C2 (Figure S29E). In addition to GGGGCC sequences, other G-rich DNA or RNA strands can form polymorphic G4s,[28] as well. For example, the conformation of human telomeric variant *htel21*_T18 (d[$(GGGTTA)_2GGGTTTGGG$]) G4 is a chair type, whereas human telomeric *htel23* (d[TA-$(GGGTTA)_3GGG$]) G4 is a hybrid type.[29,30] Nonetheless, 1D ^{1}H NMR spectra showed no apparent binding between *htel21*_T18 G4 (Figure S30A) and **cA** (1:10). Titration of **cA** (1:10) did not cause any chemical shift changes on the spectra of *htel23*_hybrid G4 (Figure S30B) or *c-kit* G4, a parallel form adopted by the *c-kit* oncogene (Figure S30C),[31] suggesting no bindings between **cA** and *htel23*_hybrid G4, or **cA** and *c-kit* G4. Other AT-rich or T-rich sequences formed structures, including an aptamer RNA hairpin form (Figure S30D), a double-stranded AT-rich DNA (Figure S30E), and a 17bp single-stranded T-rich DNA (Figure S30F), were tested through NMR titration experiments with **cA**. All of these non-G4 structures did not show any notable bindings with **cA**. Overall, these data suggest that **cA** is inclined to bind specific DNA/RNA G4C2 G4 structures, suggesting high selectivity.

DB1246, a linear, bent, positively charged molecule reminiscent of the minor-groove binder berenil, was previously reported to bind and stabilize RNA $(G4C2)_4$ G4 by other researchers.[18] Using DB1246 for comparative purposes, we found it nonselectively bound DNA $(G4C2)_4$ G4 (Figure S31A), RNA $(G4C2)_2$ G4 (Figure S31B), DNA $(G4C2)_2$ G4 (Figure S31C), and human telomeric *htel21*_T18 G4 (Figure S31D),[29,32] implying that DB1246 is a common ligand for all types of G4s.

Permeability, Cytotoxicity, and Hemolytic Activity of cA, cB, and cC. Membrane permeability, cytotoxicity, and hemolytic activity were measured to evaluate the safety margin of these compounds. Using memantine, nimodipine, and DB1246 as controls, we observed that **cA**, similar to nimodipine, showed the best permeability among these three compounds, whereas DB1246 exhibited much worse permeability than **cA**, **cB**, and **cC** (Figure 3A). Permeability of **cA** was further tested on live Neuro2a cells by treatment with different concentrations (10 or 20 μg/mL, in molar units: 16.13 or 32.26 μM) for 24 or 48 h of incubation. By analyzing supernatants of cell lysates, **cA** was detected using ultrahigh-performance liquid chromatography-mass spectrometry (UPLC-MS) in all groups, and signal intensity significantly increased in the 48 h group (Figure S32). In contrast, the intensity of the **cA** signal was the same among the three medium groups (Figure S32). These data indicate that **cA** could penetrate the cell membrane and enter cells.

To evaluate the cytotoxicity of compounds **cA**, **cB**, and **cC**, different concentrations (0.1, 1, and 10 μg/mL; in molar units, **cA**: 0.16, 1.61, 16.13 μM; **cB**: 0.16, 1.58, 15.77 μM; **cC**: 0.16, 1.57, 15.67 μM) of compounds were applied to HEK293T cells and cell viabilities were measured using the MTT assay (3-(4,5-dimethyl-2-thiazolyl)-2,5-diphenyl-2-*H*-tetrazolium bromide). No cytotoxicity of **cA** and **cC** was observed up to the concentration of 10 μg/mL (in molar units, **cA**: 16.13 μM; **cC**: 15.67 μM); however, **cB** showed apparent cytotoxicity in concentrations as low as 0.1 μg/mL (in the molar unit, 0.16 μM) (Figure 3B). Neither **cA** nor **cC** showed hemolytic activity even at 1000 μg/mL (**cA**: 1.61 mM; **cC**: 1.57 mM), but the hemolytic activity of **cB** increased in a dose-dependent manner (Figure 3C). With good permeability, low cytotoxicity, and nonhemolytic activity, these data suggest that the profile of **cA** and **cC** for a drug candidate is superior to that of **cB**.

Compounds cA and cC Rescue G4C2 EHR-Related Pathologies at the Cellular Level. Considering significant interactions with DNA/RNA G4C2 G4s (Figure 1), **cA**, **cB**, and **cC** were hypothesized to work in the same way in cells. To test, a plasmid encoding $(G4C2)_{29}$ DNA was transfected into

https://doi.org/10.1021/acs.jmedchem.2c00654
J. Med. Chem. 2022, 65, 12825−12837

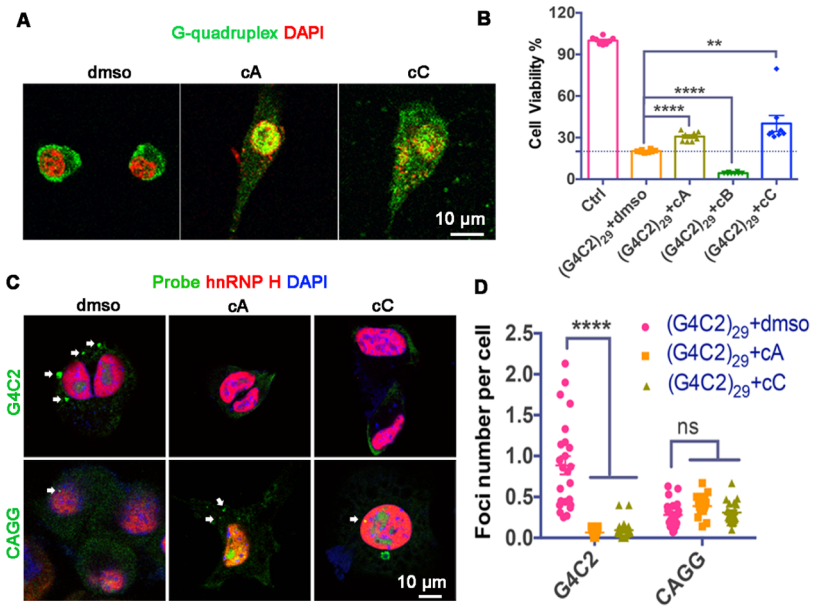

Figure 4. Compounds **cA** and **cC** rescue G4C2 EHR-related pathologies in cells. (A) Representative images of G4 antibody (green) labeled Neuro2a cells transfected with DNA $(G4C2)_{29}$ without (left) or with **cA** (1.61 μM, middle), **cC** (1.57 μM, right) treatments. DAPI was used as the counterstain (red). (B) Cell viability of **cA**, **cB**, or **cC** (1 μg/mL, in molar units, **cA**: 1.61 μM; **cB**: 1.58 μM; **cC**: 1.57 μM)-treated Neuro2a cells transfected with DNA $(G4C2)_{29}$. n = 8 batches of cell cultures; p values were determined by unpaired two-tailed t-tests. (C) Representative RNA fluorescent *in situ* hybridization (FISH) coupled hnRNP H (red) immunostaining images of Neuro2a cells transfected with DNA $(G4C2)_{29}$ and treated with **cA** (1.61 μM) or **cC** (1.57 μM). The RNA foci of G4C2 and CAGG repeats were detected with corresponding fluorescent probes (green). DAPI was used as the counterstain (blue). (D) Quantification of G4C2 and CAGG RNA foci numbers per cell in $(G4C2)_{29}$-expressing cells treated with **cA** (1.61 μM) or **cC** (1.57 μM). n = 17−25 coverslips from three batches of cell cultures; p values were determined by one-way ANOVA (Tukey's multiple comparisons test).

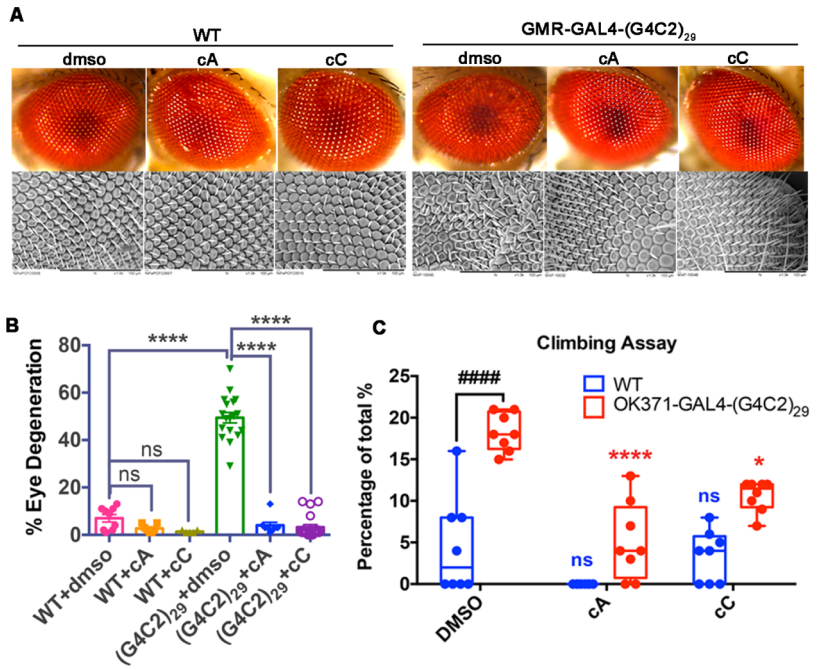

Figure 5. Compounds **cA** and **cC** rescue G4C2 EHR-related pathologies in *Drosophila*. (A) Representative external eye images (top) and scanning electron microscopy (SEM) images (bottom) of 7-day-old WT and GMR-GAL4-$(G4C2)_{29}$ *Drosophila* fed with DMSO (100 μM), compound **cA** (100 μM), or **cC** (100 μM) during the larval stage. (B) Quantification of the eye degeneration percentage of WT and GMR-GAL4-$(G4C2)_{29}$ *Drosophila* fed with DMSO (100 μM), compound **cA** (100 μM), or **cC** (100 μM). n = 7−18 animals; p values were determined by one-way ANOVA (Tukey's multiple comparisons test). (C) Climbing assay of 7-day-old WT and OK371-GAL4-$(G4C2)_{29}$ *Drosophila* fed with DMSO (100 μM), compound **cA** (100 μM), or **cC** (100 μM) during the larval stage, showing the percentage of *flies* staying at the bottom (<2 cm) of the testing tubes at the testing time of 25 s. n = 8 batches of experiments; p values were determined by one-way ANOVA (Tukey's multiple comparisons test). All data are mean ± s.e.m.

https://doi.org/10.1021/acs.jmedchem.2c00654
J. Med. Chem. 2022, 65, 12825−12837

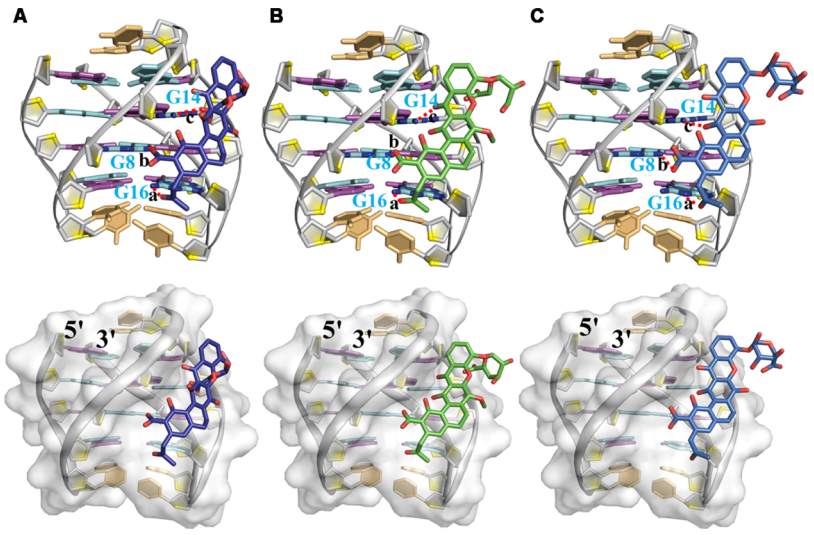

Figure 6. Structural models of DNA G4C2 G4 with **cA**, **cB**, and **cC**. Models of the predicted atomic interactions between DNA $(G4C2)_4$ G4 (PDB ID code: 2N2D; top: ribbon view, bottom: surface view) and **cA** (A, sticks view), **cB** (B, sticks view), **cC** (C, sticks view), were shown with intermolecular hydrogen bonds (red dashed lines), respectively.

Neuro2a cells as a *C9orf72* ALS/FTD cell model. Following transfections, significant cell death (>50%) was observed (Figure 4A,B). Application of either **cA** or **cC** (1 μg/mL, in molar units, **cA**: 1.61 μM; **cC**: 1.57 μM) partially rescued cell viability, whereas **cB** (1 μg/mL, 1.58 μM) made it worse (Figure 4A,B).

Expanded G4C2-repeats can be transcribed bidirectionally, leading to the formation of RNA foci, one of the primary pathologies of *C9orf72* ALS/FTD. The RNA foci then recruit specific RNA-binding proteins (RBPs), resulting in RNA processing impairment and further cytotoxicity to the central nervous system.[24,33,34] The G4C2 RNA foci colocalize with hnRNP H, forming insoluble aggregates in disease-related brain regions.[34] Having demonstrated that **cA** binds to RNA $(G4C2)_2$ G4, we next determined whether **cA** and **cC** affect G4C2 RNA foci in cells. We found that G4C2 RNA foci colocalized with hnRNP H in the $(G4C2)_{29}$-overexpressing Neuro2a cells (Figure 4C), as reported.[35] Notably, 2-day incubation with **cA** or **cC** (1 μg/mL, in molar units, **cA**: 1.61 μM; **cC**: 1.57 μM) significantly reduced G4C2 RNA foci but seldom changed CAGG RNA foci abundance (Figure 4D). These results imply that **cA** and **cC** selectively target G4C2 EHR and the downstream pathological defects in cells.

Compounds cA and cC Rescue G4C2 EHR-Related Pathologies in *Drosophila*. Moving to an *in vivo* model, we tested the protective effects of **cA** and **cC** on *C9orf72* ALS/FTD *Drosophila*. GMR-GAL4-$(G4C2)_{29}$ *Drosophila* were engineered to express $(G4C2)_{29}$ RNA exclusively in eyes; and OK371-GAL4-$(G4C2)_{29}$ *Drosophila* express $(G4C2)_{29}$ RNA exclusively in motor neurons. These mutant and wild-type (WT) *Drosophila* were fed with compounds **cA** and **cC** in a working concentration of 100 μM in solid food at the larvae stage. In the external eye assay, we noted that the eyes of 7-day-old GMR-GAL4-$(G4C2)_{29}$ adult *flies* were much rougher than age-matched WT *flies*, indicating eye degeneration (Figure 5A). The affected eye degeneration area accounted for over 50% of the whole eye (Figure 5B). Intriguingly, **cA** or **cC** treatment made eyes much smoother and more reflective (Figure 5A), significantly rescuing the rough-eye phenotype (Figure 5B). To test the impact of G4C2 EHR on the motor system, we performed a climbing assay on OK371-GAL4-$(G4C2)_{29}$ and WT *flies*. We found that the mutant *flies* remained at the bottom of the test tube to a much greater extent (18.25%) than WT *flies* (4.5%) (Figure 5C), indicating locomotor deficits. With **cA** or **cC** treatment, the percentage of bottom-staying OK371-GAL4-$(G4C2)_{29}$ *flies* decreased to 5.125 and 10.625%, respectively, significantly different from the DMSO control group, while without any changes in the climbing ability of WT *flies* (Figure 5C). These data suggest that **cA** and **cC** rescue G4C2-repeats-caused eye and motor neuron defects in *Drosophila*.

***In Silico* Molecule Docking Predicts the Binding Mode of DNA $(G4C2)_4$ G4 with cA, cB, and cC.** Knowing that the compounds interact with G4C2 G4s *in vitro* and *in vivo*, we next performed *in silico* molecule docking analysis to predict the possible interaction mode of DNA $(G4C2)_4$ G4 with **cA**, **cB**, and **cC**. As shown in Figure 6, by *in silico* analysis, **cA**, **cB**, and **cC** were predicted to interact with DNA $(G4C2)_4$ G4, which adopts an intramolecular four-layer antiparallel form. The three docking models showed that **cA**, **cB**, and **cC** perfectly fit into the wide groove between the two DNA strands of $(G4C2)_4$ G4. Three hydrogen bonds were predicted to form between G16N2 atom of DNA G4 and the O9 atom of **cA**, the G8N2 atom of DNA G4 and the O2 atom of **cA**, the G14N2 atom of DNA G4 and the O14 atom of **cA** in the interaction model of DNA G4/**cA** (Figure 6A). Similar hydrogen bonds: G16N2-**cB**O9, G8N2-**cB**O2, and G14N2-**cB**O5 were observed in the DNA G4/**cB** complex model (Figure 6B). Similarly, three hydrogen bonds: G16N3-**cC**O9, G8N2-**cC**O1, and G14N2-**cC**O4 were predicted to form in the DNA G4/**cC** docking model (Figure 6C). Notably, the estimated intermolecular energy indicated that the main contribution for the interaction complexes came from the polar interaction including van der Waals forces and hydrogen bonds, whereas the contribution from electrostatic interaction was relatively low (Table S10).

Compounds cA, cB, and cC Target Cellular ROS. Enhanced microglial activation is regarded as one of the primary characteristics of ALS/FTD patients with C9ORF72 mutations.[36] The activated microglia could release reactive

https://doi.org/10.1021/acs.jmedchem.2c00654
J. Med. Chem. 2022, 65, 12825−12837

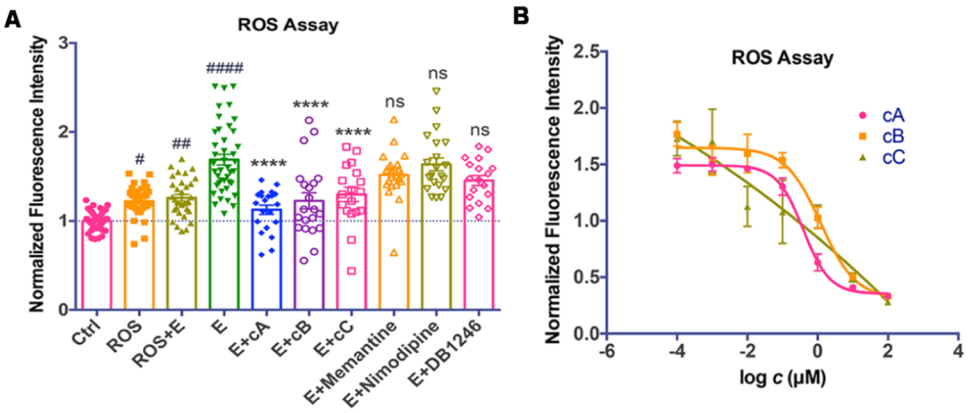

Figure 7. ROS assay of **cA, cB, and cC**. (A) Cellular ROS levels in different treatment groups. n = 18−42 wells from three batches of cell cultures; p values were determined by one-way ANOVA (Tukey's multiple comparisons test); # indicates the comparison to the control (ctrl) group; * indicates the comparison to E group. All data are mean ± s.e.m. (B) Dose−response curves (x: log concentration, y: normalized ROS fluorescence intensity) of **cA**, **cB**, and **cC** on scavenging cellular ROS tested on differentiated HT22 cell cultures pretreated with 5 mM L-glutamate. n = 3 independent preparations.

oxygen species (ROS), which are toxic to neurons, thus accelerating neuronal death.[36] Considering the multiple phenolic hydroxy groups in the structures of compounds **cA**, **cB**, and **cC**, we hypothesized that these multiple phenolic hydroxy groups might protect cells from oxidative stress, such as insults from cellular ROS. Tests in HT22 cells revealed that **cA**, **cB**, and **cC** significantly decreased the cellular ROS levels induced by glutamate in a dose−response manner (Figure 7), suggesting that **cA** and **cC** might protect differentiated HT22 cells by removing excessive cellular ROS. In contrast, memantine, nimodipine, and DB1246 showed no obvious effects on scavenging ROS (Figure 7A). These results indicate that the ROS-scavenging ability may also contribute to the neuroprotective activity of **cA** and **cC**.

■ DISCUSSION AND CONCLUSIONS

G4C2 EHR in the first intron of the *C9orf72* gene is the most dominant genetic cause of ALS and FTD.[6,7] *C9orf72* DNA and RNA EHR could form noncanonical secondary structures, G-quadruplexes (G4s);[8,9] therefore, *C9orf72* G4s become attractive targets for drug development. Here, compound **cA** was proved to be able to selectively bind DNA $(G4C2)_4$ G4 (Figure 1A) and RNA $(G4C2)_2$ G4 (Figure 1C). In contrast, no binding phenomenon was observed on the titration of **cA** to DNA two-repeat G4C2 formed G4 (Figure S29A), double-stranded DNA G4C2 (Figure S29B), single-stranded two-repeat DNA G4C2 (Figure S29C), four-repeat RNA G4C2 hairpin form (Figure S29D), double-stranded RNA G4C2 (Figure S29E), human telomeric G4s (*htel21*_T18 and *htel23*_hybrid) (Figure S30A,B), *c-kit* G4 (Figure S30C), aptamer RNA hairpin form (Figure S30D), double-stranded AT-rich DNA (Figure S30E), and single-stranded T-rich DNA (Figure S30F), suggesting the high selectivity of **cA**. Furthermore, *in silico* molecule docking analysis showed that **cA**, **cB**, and **cC** perfectly fit into the wide groove between two DNA strands of $(G4C2)_4$ G4, which adopts an intramolecular four-layer antiparallel form (Figure 6).[9,37] Three hydrogen bonds were predicted to form between G16(a), G8(b), G14(c), and hydroxyl radical groups of **cA**, **cB**, and **cC** in the docking models (Figure 6). Notably, the binding sites of these compounds on the $(G4C2)_4$ G4 shown in models are consistent with the chemical shift changes observed in the NMR titration experiments (Figure 1A). Altogether, these data indicate that the marine natural products **cA**, **cB**, and **cC** can selectively recognize *C9orf72* G4C2 G4s. In contrast, DB1246, a linear, bent, positively charged molecule reminiscent of the minor-groove binder berenil, was previously shown to stabilize and bind DNA and RNA G4C2 G4s.[18] Nevertheless, we found that DB1246 showed strong bindings not only to DNA $(G4C2)_4$ G4 (Figure S31A), and RNA $(G4C2)_2$ G4 (Figure S31B) but also to DNA $(G4C2)_2$ G4 (Figure S31C) and human telomeric G4 (*htel21*_T18) (Figure S31D); therefore, it might be a common ligand for all types of G4 structures without selectivity. These data provide evidence that **cA** is an exceptional selective G4C2 G4-binding molecule, which shows great potential as a good therapeutic candidate for *C9orf72* ALS/FTD disease worthy of further clinical evaluations.

Differences in pharmacological properties and bioactivity of these three structure-similar natural compounds are compelling. Intriguingly, **cA** and **cC** showed no hemolytic activity with a pretty high concentration of 1000 μg/mL (in molar units, **cA**: 1.61 mM; **cC**: 1.57 mM), while **cB** showed significant hemolytic activity starting at 500 μg/mL (0.79 mM) in a dose-dependent manner (Figure 3C). Also, in the $(G4C2)_{29}$-expressing cells, **cC** enhanced the cell viability from 20 to 40%, and a 30% increase was observed in the **cA** treated group (Figure 4B). However, the **cB**-treated group was even worse than the model group, indicating potent cytotoxicity instead of protection against cell death. The intrinsic cause of their bioactivity differences could be attributed to their structural differences. The hydroxyl group in C-17 might be crucial; though the hydrophobic methoxyl group introduction does not influence the binding affinity to G4s as the methoxyl group points out to solvent, it does increase the cytotoxicity of **cB**. Compared with its dehydrated product **cA**, **cC** exhibited better neuroprotective activity and binding affinity to G4s. Therefore, the underlying structure−activity relationship is worthy of further investigation.

To the best of our knowledge, this study is the first to uncover new chemical structures of the three marine natural products discussed above with neuroprotective activity. Structures with similar skeletons reported previously by others show various bioactivities, including antiproliferative,[38−40] antibacterial,[38,40,41] and antioxidant activities.[42] Remarkably, two hexaricins with a similar hexacyclic xanthone skeleton as

https://doi.org/10.1021/acs.jmedchem.2c00654
J. Med. Chem. 2022, 65, 12825−12837

our compounds show strong antioxidant activities in scavenging free radicals.[42] Edaravone, the ALS drug approved by the United States in 2017, is a potent antioxidant agent to eliminate hydroxyl radicals and lipid peroxides in neurons.[4] Based on the ROS assay, **cA**, **cB**, and **cC** were observed to dramatically reduce cellular ROS levels in a dose−response manner (Figure 7), providing another reasonable explanation for their neuroprotective mode of action.

Three underlying mechanisms of *C9orf72* ALS/FTD pathogenesis have been proposed: (1) loss of function of the *C9orf72* gene, (2) toxic RNA foci by RBPs and RNA G4C2 EHR, and (3) toxic dipeptides from RAN translation.[23,24] Our findings indicate that the neuroprotective activity of **cA** and **cC** is probably attributed to their specific bindings to DNA $(G4C2)_4$ G4 and RNA $(G4C2)_2$ G4, therefore protecting neuronal cells from G4C2 G4s-related pathologies. Also, **cA** and **cC** can fight against the insults from cellular ROS. However, it remains to be seen whether **cA** or **cC** could protect neuronal cells from toxic DPR proteins. To conclude, compounds **cA** and **cC** might play their neuroprotective roles by targeting G4C2 G4s or related downstream factors contributing to *C9orf72* ALS/FTD pathologies, including (1) G4C2 DNA EHR-mediated C9ORF72 insufficiency, (2) G4C2 RNA foci-caused toxicity, (3) cellular ROS insults. Detailed working mechanisms of **cA** and **cC** warrant further investigation in the future.

EXPERIMENTAL SECTION

Sample Preparation of DNA/RNA G4s. Single DNA/DNA strands were purchased from Integrated DNA Technologies and Takara. The single-strand DNA/RNA sample at 100 μM was annealed by heating up to 95 °C for 15 min and slowly cooled to room temperature in the annealing buffer (70 mM KCl, 20 mM potassium phosphate, pH 7.0) overnight. The final NMR samples contained 0.1 mM DNA or RNA in 70 mM KCl and 20 mM potassium phosphate buffer (pH 7.0).

One-Dimensional (1D) ^{1}H Nuclear Magnetic Resonance (NMR) Titration. The 1D ^{1}H NMR spectra were performed at 25 °C. All compounds were dissolved in isotope-labeled DMSO-d_6 (Sigma-Aldrich) at about 50 mM concentration, working as stock solutions. DMSO-d_6 (10 μL) was added into 500 μL of 0.1 mM DNA/RNA G4 solution in the NMR buffer (70 mM KCl, 20 mM potassium phosphate, pH 7.0, 10% D_2O) to avoid chemical shift changes in DNA/RNA G4 resulting from DMSO-d_6 addition. Then, 1D ^{1}H NMR spectrum was recorded as a reference. During NMR titration experiments of adding each compound into the DNA/RNA G4 solution, the maximal volume of 10 μL of each compound in the DMSO-d_6 solution was regarded as a final data point. All used sequences of the secondary structures for the 1D ^{1}H NMR titration experiments are listed in Table S11.

Fluorescence Intensity Assay. 3′-FAM-labeled DNA $(G4C2)_4$ G4 or RNA $(G4C2)_2$ G4 was synthesized from BGI-Hongkong Co Ltd. It was heated at 98 °C for 10 min in 10 mM K^+ solution (8 mM KCl, 2 mM KH_2PO_4 at pH 6.8) with a final concentration of 1 μM, followed by slowly cooling down to room temperature. **cA**, **cB**, or **cC** was added together with the 3′-FAM-labeled DNA $(G4C2)_4$ G4 or RNA $(G4C2)_2$ G4 in the same buffer at different concentrations. The fluorescence intensity spectrum was collected by a FlexStation 3 Multi-Mode Microplate Reader at room temperature with an excitation/emission wavelength of 470/520 nm. Fluorescence intensity and the concentration of **cA**, **cB**, or **cC** were used for binding affinity (K_D) calculation by fitting these data into nonlinear regression at one site (specific binding with Hill slope) mode using Prism 6 software.

Strains. The *S. chrestomyceticus* strain was purchased from Thailand Bioresource Research Center.

Fermentation, Extraction, and Isolation. The *S. chrestomyceticus* strain was cultured in two 125 mL Erlenmeyer flasks containing 50 mL of the glucose, yeast, and malt (GYM) medium (4 g of yeast extract, 10 g of malt extract, and 4 g of D-glucose per liter of distilled water) and 20−30 glass beads (3 mm in diameter) at 30 °C with an agitation of 180 rpm for 3 days. Then, 1% of the seed broth was transferred into 10 Erlenmeyer flasks containing 1 L of the GYM media with around 100 glass beads at 30 °C with an agitation of 180 rpm for 10 days of fermentation. The bacterial culture broth was extracted with an equal volume of ethyl acetate three times to obtain crude extract. The crude extract was separated by reversed-phase C18 column chromatography and eluted with 20, 40, 60, 80, and 100% acetonitrile to obtain different fractions. Compounds **cA**, **cB**, and **cC** were obtained in the 60% eluate monitored at an ultraviolet (UV) wavelength of 210 nm (Waters 2998 Photodiode Array Detector) and further purified through semipreparative high-performance liquid chromatography (HPLC, Waters 2695 Separations Module; Milford) using a Phenomenex Luna C18 column, 250 mm × 10 mm in size, and designed for a particle size of 5 μm. Pure fractions were eluted with an isocratic mobile phase at a flow rate of 3 mL/min (solution A: acetonitrile with 0.5‰ trifluoroacetic acid (TFA); solution B: Milli-Q water with 0.5‰ TFA. Acetonitrile/water ratio was 30%) and monitored at a UV wavelength of 210 nm (Waters 2998 Photodiode Array Detector). Compounds were collected, freeze-dried by Labconco FreeZone 4.5 L Benchtop Freeze Dry System, dissolved in DMSO, and stored at −20 °C for further biological assessments or long-term storage.

Structural Elucidation. All compounds are >95% pure by HPLC. MS data were recorded from a Bruker ultrafleXtreme ultrahigh-resolution TOF LC-MS system and a matrix-assisted laser desorption/ionization-time-of-flight (MALDI-TOF)/TOF Mass Spectrometer (Bruker Daltonics). Optical rotations were determined using a Jasco P-2000 Polarimeter. ^{1}H and ^{13}C NMR spectra were performed on 800 and 200 MHz Varian spectrometers, respectively. All standard 2D NMR experimental spectra, including NOESY, HSQC, HMBC, and COSY, were collected at 25 °C.

Crystallization and X-ray Crystallography. The crystallization of **cA** was achieved by solvent diffusion of an acetonitrile-methanol solution over several days. Single-crystal X-ray data were collected on a Rigaku OD Supernova instrument (Cu Kα radiation) at −173.15 °C. A thin yellow plate (0.2 mm × 0.08 mm × 0.02 mm) was immersed in Paratone and mounted in a cryo-loop on a Rigaku-Oxford Diffraction Supernova diffractometer, and diffraction data were collected at −173.15 °C. The resulting monoclinic crystal structure was refined successfully to a conventional R1 = 5.98% with a residual electron density peak/hole of +0.26/−0.29 e/Å^3 and a Flack handedness parameter of 0.1. This result revealed the **cA** skeleton with a 4,5-dehydro-D-glucuronic acid moiety at one end (sugar C2′ = R, C3′ = S), a central hydroquinone-xanthone unit, and a disordered arrangement between the open and cyclic forms at the other end, representing isomers that are in solution equilibrium. A 50:50 disorder in the crystal is required because of the potential overlap of groups in neighboring molecular pairs. Hence, an open form is in close contact with a cyclic form. The structural arrangement of the two disordered molecular fragments refines geometrically sensibly without the need for severe restraints. The cyclic form is an α-hydroxylactone with an R-stereochemical center. The open form, which is indicated in forming a supramolecular association with the quadruplex, has exocyclic carboxylic acid (−COOH) and acetonyl (−CH2-COMe) groups. The structure contains several water and methanol molecules that are also partially disordered due to disorders in the central molecule.

Parallel Artificial Membrane Permeability Assay. Test compound (500 μL, 500 μM) and Equilibrium Standards (500 μL, 200 μM) for each test compound were prepared. DMSO (5 μL) plus phosphate-buffered saline (PBS, 245 μL) served as blank control. First, 300 μL of PBS was added to each well in the acceptor plate. With the donor plate in its tray, 5 μL of 4% lecithin in dodecane was added directly to the well membranes of the donor plate. Each 500 μM test compound (200 μL) was added to duplicate wells of the

https://doi.org/10.1021/acs.jmedchem.2c00654
J. Med. Chem. 2022, 65, 12825−12837

donor plate. The donor plate was carefully placed into the acceptor plate wells and incubated at 37 °C for 18 h. Then, the liquid in acceptor plate wells was collected as acceptor solution for analysis. The absorbance spectrum from 200 to 500 nm in 10 nm intervals was read to determine the peak absorbance of test compounds and blank control.

Cell Culture. HEK293T, Neuro2a, and HT22 cells (Sigma-Aldrich, SCC129) were cultured in Dulbecco's modified Eagle's medium (DMEM, Thermo Fisher Scientific, 11965092) with 10% fetal bovine serum (FBS; Thermo Fisher Scientific, 26140079) plus penicillin−streptomycin (Thermo Fisher Scientific, 15140163; 10,000 U/mL) at 37 °C in a humidified incubator with an atmosphere of 5% CO_2 and 95% air.

MTT Assay. Cytotoxicity of compounds was tested by MTT assay. Cells were grown in DMEM (Gibco) with 10% FBS and 1% penicillin−streptomycin at 37 °C with 5% CO_2. In total, 5×10^3 cells were seeded in each well of 96-well plates and cultured for 24 h. Then, the cells were treated with different concentrations of compounds dissolved in DMSO for another 24 h. After incubating with 20 μL of MTT (5 mg/mL, in the molar unit: 12.07 mM) for each well at 37 °C for another 4 h, 100 μL of DMSO was added to dissolve formazan. Absorbance was measured using a Multiskan FC microplate photometer at 570 nm. IC_{50} data were analyzed with GraphPad Prism software.

Hemolysis Assay. Hemolytic activity was determined with 2% fresh red blood cells from a healthy rabbit. Blood cells were obtained and washed with PBS four to five times and centrifuged at 1500 rpm for 10 min until the upper phase became clear. Compounds were diluted with PBS to final concentrations of 1000, 500, and 250 μg/mL (in molar units, **cA**: 1.61, 0.81, 0.40 mM; **cB**: 1.58, 0.79, 0.39 mM; **cC**: 1.57, 0.78, 0.39 mM, respectively), added to the same volume of 2% red blood cells, and incubated at 37 °C for 1 h. Samples were centrifuged at 10,000 rpm for 5 min, and supernatants were added to 96-well plates and measured at 570 nm with a Thermo Scientific Multiskan FC multiplate photometer (Thermo Scientific). An aliquot of 10% Triton X-100 was used as the positive control, and 1% DMSO dissolved in PBS was used as the negative control.

Transfection. DNA constructs were transfected to neuronal Neuro2a cell lines using Lipofectamine 2000 (Thermo Fisher Scientific, 11668019). At 4−6 h after transfection, a fresh culture medium was used to replace the transfection medium, and cells were incubated for another 48 h to allow recovery and construct expression.

RNA Fluorescent *In Situ* Hybridization and Immunocytochemistry. Neuro2a cells planted on coverslips were transfected with a pHR-Tre3G-29xGGGGCC-12xMS2 plasmid (#99149), incubated for 2−3 days, and then fixed with 4% paraformaldehyde for 15 min at room temperature. The cells were permeabilized with 0.1% Triton X-100 in PBS for 10 min before hybridization. Target probe (GGCCCCGGCCCCGGCCCCGGCCCC) with a 5′-Cy3 and control probe (CAGGCAGGCAGGCAGGCAGG) with a 5′-Cy5 were added to the hybridization solution (0.9 M NaCl, 0.02 M Tris−HCl, 0.01% SDS, 20% formamide). The cells were then incubated in the mixed solution at 46 °C for 3 h. The cells were washed three times in washing solution (0.02 M Tris−HCl, 0.001% SDS, 5 mM EDTA) at 48 °C, 15 min each time. Then, the cells were stained with primary antibodies (Anti-DNA G-quadruplex (G4) antibody (Cat. No. MABE1126) or Anti-hnRNP H antibody (ab10374)) at 1:500 dilution and incubated at 4 °C overnight. The next day, the cells were washed three times with PBS (10 min each time) and then incubated with secondary antibodies (Alexa 488 anti-mouse for G4 or Alex 488 anti-rabbit for hnRNP H) at 1:500 dilution for 1 h at room temperature. Superfluous secondary antibodies were washed away with PBS three times (10 min each time). Then, the cells were incubated with DAPI at 1:5000 dilution for 5 min and washed with PBS once. Finally, the cells on slides were air-dried, mounted in a Hydromount medium, and analyzed by confocal microscopy (Leica, SP8).

***Drosophila* Feeding.** *Fly* lines expressing 29 GGGGCC repeats (29R) under the GMR-GAL4 promoter (GMR-GAL4-$(G4C2)_{29}$) and OK371-GAL4 promoter (OK371-GAL4-$(G4C2)_{29}$) were purchased from Bloomington Drosophila Stock Center. All *flies* were raised at room temperature (25 °C) on a cornmeal medium supplemented with dry yeast. DMSO served as the vehicle control, and **cA** and **cC** were added at a working concentration of 100 μM, respectively. Parent *flies* for cross were set in solid food containing testing compound, and F1 *larvae* were fed with food continuously until eclosion. After eclosion, F1 *flies* were transferred to regular food containers without compounds. The animal protocol (AEP-2021-0089) was approved by the Animal Ethics Committee at HKUST, and animal care was in accordance with both institutional and Hong Kong guidelines that include government legislation, Hong Kong's Code of Practice for Care and Use of Animals for Experimental Purposes, as well as International Guides and Codes of Practice on the Care and Use of Animals in Research.

External Eye Assay. Eye images of GMR-GAL4-$(G4C2)_{29}$ or WT adult *flies* on day 7 after eclosion were captured using a charge-coupled device (CCD) camera on an Olympus stereomicroscope. Eye morphologies of *flies* in different treatment groups were compared to evaluate the retina degeneration level. The affected eye area and total eye area were measured to calculate the degeneration ratio by ImageJ.

Scanning Electron Microscopy (SEM) Imaging. Adult *Drosophila* was anesthetized by CO_2, and the head was immediately dissected from the body under a stereomicroscope. Head samples were fixed with 4% (v/v) glutaraldehyde for 24 h at room temperature and washed with PBS three times after fixation. After that, the samples were dehydrated in gradient ethanol solutions (30, 50, 70, 90% v/v with Milli-Q water, and three times with 100% ethanol, 10 min for each step) followed by 4 h air drying. Samples were then coated with a gold layer by a Magnetron Ion Sputter Device MSP-2S before imaging. SEM images were taken under a Hitachi TM3030 Tabletop Scanning Electron Microscope.

***Drosophila* Climbing Assay.** The climbing ability was analyzed by negative geotaxis. For each test, at least 15 *flies* were placed into a vertical plastic column and anesthetized. After recovery for 1 h, *flies* were tapped to the bottom. The percentage of *flies* that climb from the bottom of the column (>2 cm) at 25 s was used to estimate climbing ability. The interval between each experiment was 3 min; a total of three trials were performed.

Molecule Docking. Docking, energy filtering, clustering, and ranking of DNA $(G4C2)_4$ G4-**cA**, DNA $(G4C2)_4$ G4-**cB**, and DNA $(G4C2)_4$ G4-**cC** were performed using AutoDock4.2.[43] The NMR structure of DNA $(G4C2)_4$ G4 (PDB code: 2N2D) was obtained from the Protein Data Bank (PDB). Both the DNA and compound structures were converted to AutoDock4.2 format files using AutoDockTools (1.5.6),[44] and the Gesteiger−Marsili partial charges were then assigned to the atoms of the compound and DNA. The Lamarckian Genetic algorithm was applied, and 150 separate dockings with a maximum of 1.75×10^6 energy evaluations were performed. During the docking procedure, DNA structure was regarded as rigid, whereas ligand molecules were considered flexible. Finally, the conformation with the lowest binding free energy of the most populated cluster member was selected as the most probable binding conformation. PyMOL was used to analyze the potential presence of interacting bonds of the most favorable confirmation obtained from AutoDock4.2.

Reactive Oxygen Species (ROS) Assay. Cultured HT22 cells were differentiated by applying 10 μM retinoic acid (Sigma-Aldrich, R2625-50MG) and 500 μM cyclic adenosine monophosphate (cAMP, Sigma-Aldrich, A6885) in DMEM medium supplied with 0.5% FBS (differentiation medium) and incubated for 48 h before adding other treatments. L-Glutamate acid at 5 mM was applied for 24 h of incubation. Then, the 2′-7′dichlorofluorescin diacetate (DCFH-DA) fluorescent probe was added to cells in DMEM-only medium at 10 μM working concentration for a total of 30 min incubation with gentle shaking every 5 min at 37 °C. After removing the fluorescent probe, the cells were washed with probe-free DMEM-only medium three times to wash away redundant probe. Tested compounds (**cA**, **cB**, **cC**: 2 μg/mL, in molar units, **cA**: 3.23, **cB**: 3.15, **cC**: 3.13 μM), other control drugs (memantine, nimodipine, DB1246:

https://doi.org/10.1021/acs.jmedchem.2c00654
J. Med. Chem. 2022, 65, 12825−12837

2 μM), and positive ROS control (Rosup: 50 μg/mL) were then applied to different wells of cells for 1 h of incubation. The fluorescence intensity of dichlorofluorescein (DCF), oxidated from DCFH by cellular ROS, was then measured using a microplate reader with 488/525 nm excitation/emission filters.

Circular Dichroism (CD) Spectroscopy and Melting Experiment. CD spectra of G4s or G4s with compounds were recorded on an Applied Photophysics Chirascan CD spectrometer at 25 °C using a 1 mm path length quartz cuvette with a sample volume of 400 μL. Each G4 sample was prepared at a concentration of 15 μM. The compounds were mixed with G4 at a molar ratio of 1:10. An average of three scans was taken, and the spectrum of the buffer was subtracted. The CD melting experiments were performed in the temperature range of 25−95 °C using a temperature heating rate of 1 °C/min. The CD absorbance was measured at a single wavelength following the normalization using the equation (Abst − min)/(max − min). Abst is the absorbance at a given temperature, max is the maximum absorbance at 260 nm for RNA G4 (a parallel form) and 290 nm for DNA G4 (an antiparallel form), and min is the minimum value. All data were fitted by the Boltzmann sigmoid equation using Prism.

Statistical Analysis. All data were obtained from at least three independent preparations. Quantifications were performed in a blinded manner. Statistical analysis was performed with GraphPad Prism 6. Differences between groups were analyzed using the unpaired *t*-test. Statistical significance was considered at $p \leq 0.05$.

■ ASSOCIATED CONTENT

Supporting Information

The Supporting Information is available free of charge at https://pubs.acs.org/doi/10.1021/acs.jmedchem.2c00654.

Figure S1−S32; Table S1−S12; refinement model description (PDF)

PDB ID of New Crystal (X-ray) Structures/Homology Models: DNA (G4C2)4 G4 (PDB code: 2N2D) was obtained from the Protein Data Bank (PDB). Three-dimensional crystal structures of compound **cA** were deposited to the Cambridge Structural Database with deposition number 2082249

g4c2-**cA** (PDB)

g4c2-**cB** (PDB)

g4c2-**cC** (PDB)

SMILE (CSV)

X-ray data of **cA** (CIF)

■ AUTHOR INFORMATION

Corresponding Authors

Guang Zhu − *Division of Life Science and State Key Laboratory of Molecular Neuroscience, The Hong Kong University of Science and Technology, Hong Kong 999077, China; Shenzhen Research Institute, The Hong Kong University of Science and Technology, Shenzhen 518057, China;* orcid.org/0000-0003-3802-3446; Email: gzhu@ust.hk

Pei-Yuan Qian − *Department of Ocean Science and Hong Kong Branch of Southern Marine Science and Engineering Guangdong Laboratory (Guangzhou), The Hong Kong University of Science and Technology, Hong Kong 999077, China; Southern Marine Science and Engineering Guangdong Laboratory (Guangzhou), Guangzhou 511458, China;* Email: boqianpy@ust.hk

Authors

Aifang Cheng − *Department of Ocean Science and Hong Kong Branch of Southern Marine Science and Engineering Guangdong Laboratory (Guangzhou), The Hong Kong University of Science and Technology, Hong Kong 999077, China; Southern Marine Science and Engineering Guangdong Laboratory (Guangzhou), Guangzhou 511458, China;* orcid.org/0000-0002-5022-418X

Changdong Liu − *Division of Life Science and State Key Laboratory of Molecular Neuroscience, The Hong Kong University of Science and Technology, Hong Kong 999077, China; Shenzhen Research Institute, The Hong Kong University of Science and Technology, Shenzhen 518057, China*

Wenkang Ye − *Department of Ocean Science and Hong Kong Branch of Southern Marine Science and Engineering Guangdong Laboratory (Guangzhou), The Hong Kong University of Science and Technology, Hong Kong 999077, China; Southern Marine Science and Engineering Guangdong Laboratory (Guangzhou), Guangzhou 511458, China; SZU-HKUST Joint Ph.D. Program in Marine Environmental Science, Shenzhen University, Shenzhen 518060, China*

Duli Huang − *Department of Ocean Science and Hong Kong Branch of Southern Marine Science and Engineering Guangdong Laboratory (Guangzhou), The Hong Kong University of Science and Technology, Hong Kong 999077, China; Southern Marine Science and Engineering Guangdong Laboratory (Guangzhou), Guangzhou 511458, China*

Weiyi She − *Department of Ocean Science and Hong Kong Branch of Southern Marine Science and Engineering Guangdong Laboratory (Guangzhou), The Hong Kong University of Science and Technology, Hong Kong 999077, China; Southern Marine Science and Engineering Guangdong Laboratory (Guangzhou), Guangzhou 511458, China; SZU-HKUST Joint Ph.D. Program in Marine Environmental Science, Shenzhen University, Shenzhen 518060, China*

Xin Liu − *Department of Ocean Science and Hong Kong Branch of Southern Marine Science and Engineering Guangdong Laboratory (Guangzhou), The Hong Kong University of Science and Technology, Hong Kong 999077, China; Southern Marine Science and Engineering Guangdong Laboratory (Guangzhou), Guangzhou 511458, China*

Chun Po Fung − *Division of Life Science and State Key Laboratory of Molecular Neuroscience, The Hong Kong University of Science and Technology, Hong Kong 999077, China*

Naining Xu − *Division of Life Science and State Key Laboratory of Molecular Neuroscience, The Hong Kong University of Science and Technology, Hong Kong 999077, China; Department of Oral and Maxillofacial Surgery, Stomatological Center, Peking University Shenzhen Hospital, Shenzhen Peking University-The Hong Kong University of Science and Technology Medical Center, Shenzhen 518036, China*

Monica Ching Suen − *Division of Life Science and State Key Laboratory of Molecular Neuroscience, The Hong Kong University of Science and Technology, Hong Kong 999077, China*

Wei Ye − *Department of Ocean Science and Hong Kong Branch of Southern Marine Science and Engineering Guangdong Laboratory (Guangzhou), The Hong Kong University of Science and Technology, Hong Kong 999077, China; Southern Marine Science and Engineering Guangdong Laboratory (Guangzhou), Guangzhou 511458, China*

Herman Ho Yung Sung − *Department of Chemistry, The Hong Kong University of Science and Technology, Hong Kong 999077, China*

Ian Duncan Williams − *Department of Chemistry, The Hong Kong University of Science and Technology, Hong Kong 999077, China*

Complete contact information is available at: https://pubs.acs.org/10.1021/acs.jmedchem.2c00654

Author Contributions

○A.C., C.L., and Wenkang Y. contributed equally to this work. A.C. contributed to conceptualization, methodology, investigation, visualization, writing—original draft, writing—revisions & editing review. C.L. contributed to methodology, investigation, visualization, grant acquisition, and writing—editing review. Wenkang Y. involved in methodology, investigation, and visualization. D.H., W.S., X.L., C.P.F., N.X., M.C.S., and Wei Y. performed investigation. H.H.Y.S. contributed to methodology and visualization. I.D.W. contributed to methodology, visualization, and supervision. G.Z. involved in methodology, supervision, grant acquisition, and writing—review & editing review. P.-Y.Q. contributed to conceptualization, methodology, supervision, grant acquisition, and writing—review & editing review.

Notes

The authors declare the following competing financial interest(s): This work has been submitted for the U.S. patent application (no. 17/447,784) and Chinese patent application (no. 202111078152.X). The authors declare no other conflicts of interest.

■ ACKNOWLEDGMENTS

This study was supported by National Key R & D Program of China (2018YFA0903200 to P.-Y.Q.), Hong Kong Branch of Southern Marine Science and Engineering Guangdong Laboratory (Guangdong) (SMSEGL20SC01 to P.-Y.Q.), General Research Found from the Research Grants Council of HKSAR government (16100722 to A.C.), CRF grant from the HKSAR government (C6026-19G-A to P.-Y.Q.), Key Special Project for Introduced Talents Team of Southern Marine Science and Engineering Guangdong Laboratory (Guangzhou) (GML2019ZD0409 to P.-Y.Q.), National Natural Science Foundation of China (32071188 to C.L.), Hong Kong Special Administrative Region (16103719, 16101120, 16101121, SZSTI19SC02, SMSEGL20SC01-H, AoE/M-403-16, AoE/M-401/20, VPRDO19RD03-6 to G.Z.), and Guangdong Basic and Applied Basic Research Foundation (2020A1515010034 to C.L.). The authors thank Prof. Yan Yan and Miss Ying Wang from the Division of Life Science, the Hong Kong University of Science and Technology (HKUST), for their help and support on *Drosophila*-related experiments, and also thank Rui Feng from the Division of Life Science, HKUST, for his help on NMR experiments.

■ ABBREVIATIONS USED

1D, one-dimensional; ALS, amyotrophic lateral sclerosis; BBB, blood−brain barrier; **cA**, chrexanthomycin A; cAMP, cyclic adenosine monophosphate; **cB**, chrexanthomycin B; **cC**, chrexanthomycin C; CCD, charge-coupled device; CD, circular dichroism; COSY, H−H correlation spectroscopy; DCF, dichlorofluorescein; DCFH-DA, 2′-7′dichlorofluorescin diacetate; DMEM, Dulbecco's modified Eagle's medium; DMSO, dimethyl sulfoxide; DPR, dipeptide repeat; EHR, expanded hexanucleotide repeat; FBS, fetal bovine serum; FTD, frontotemporal dementia; G4, G-quadruplex; G4C2, GGGGCC; GYM, glucose, yeast, and malt; HKUST, Hong Kong University of Science and Technology; HMBC, ^{1}H detected heteronuclear multiple bond correlation; HPLC, high-performance liquid chromatography; HRMS, high-resolution mass spectrometry; HSQC, heteronuclear single quantum coherence; K_D, binding affinity; MALDI-TOF, matrix-assisted laser desorption/ionization-time of flight; MTT, 3-(4,5-dimethyl-2-thiazolyl)-2,5-diphenyl-2-*H*-tetrazolium bromide; NMR, nuclear magnetic resonance; NOESY, nuclear Overhauser enhancement spectroscopy; PBS, phosphate-buffered saline; PDB, protein data bank; RAN, repeat-associated non-ATG; RBPs, RNA-binding proteins; ROS, reactive oxygen species; SEM, scanning electron microscopy; TFA, trifluoroacetic acid; UPLC-MS, ultrahigh-performance liquid chromatography-mass spectrometry; UV, ultraviolet; WT, wild-type

■ REFERENCES

(1) Hardiman, O.; Al-Chalabi, A.; Chio, A.; Corr, E. M.; Logroscino, G.; Robberecht, W.; Shaw, P. J.; Simmons, Z.; van den Berg, L. H. Amyotrophic lateral sclerosis. *Nat. Rev. Dis. Primers* **2017**, *3*, No. 17071.

(2) Brown, D. G.; Shorter, J.; Wobst, H. J. Emerging small-molecule therapeutic approaches for amyotrophic lateral sclerosis and frontotemporal dementia. *Bioorg. Med. Chem. Lett.* **2020**, *30*, No. 126942.

(3) Dharmadasa, T.; Kiernan, M. C. Riluzole, disease stage and survival in ALS. *Lancet Neurol.* **2018**, *17*, 385−386.

(4) Dorst, J.; Ludolph, A. C.; Huebers, A. Disease-modifying and symptomatic treatment of amyotrophic lateral sclerosis. *Ther. Adv. Neurol. Disord.* **2018**, *11*, No. 1756285617734734.

(5) Oskarsson, B.; Gendron, T. F.; Staff, N. P. Amyotrophic lateral sclerosis: an update for 2018. *Mayo Clin. Proc.* **2018**, *93*, 1617−1628.

(6) DeJesus-Hernandez, M.; Mackenzie, I. R.; Boeve, B. F.; Boxer, A. L.; Baker, M.; Rutherford, N. J.; Nicholson, A. M.; Finch, N. A.; Flynn, H.; Adamson, J.; Kouri, N.; Wojtas, A.; Sengdy, P.; Hsiung, G.Y.R.; Karydas, A.; Seeley, W. W.; Josephs, K. A.; Coppola, G.; Geschwind, D. H.; Wszolek, Z. K.; Feldman, H.; Knopman, D. S.; Petersen, R. C.; Miller, B. L.; Dickson, D. W.; Boylan, K. B.; Graff-Radford, N. R.; Rademakers, R. Expanded GGGGCC hexanucleotide repeat in noncoding region of C9ORF72 causes chromosome 9p-linked FTD and ALS. *Neuron* **2011**, *72*, 245−256.

(7) Renton, A. E.; Majounie, E.; Waite, A.; Simon-Sanchez, J.; Rollinson, S.; Gibbs, J. R.; Schymick, J. C.; Laaksovirta, H.; van Swieten, J. C.; Myllykangas, L.; Kalimo, H.; Paetau, A.; Abramzon, Y.; Remes, A. M.; Kaganovich, A.; Scholz, S. W.; Duckworth, J.; Ding, J. H.; Harmer, D. W.; Hernandez, D. G.; Johnson, J. O.; Mok, K.; Ryten, M.; Trabzuni, D.; Guerreiro, R. J.; Orrell, R. W.; Neal, J.; Murray, A.; Pearson, J.; Jansen, I. E.; Sondervan, D.; Seelaar, H.; Blake, D.; Young, K.; Halliwell, N.; Callister, J. B.; Toulson, G.; Richardson, A.; Gerhard, A.; Snowden, J.; Mann, D.; Neary, D.; Nalls, M. A.; Peuralinna, T.; Jansson, L.; Isoviita, V. M.; Kaivorinne, A. L.; Holtta-Vuori, M.; Ikonen, E.; Sulkava, R.; Benatar, M.; Wuu, J.; Chio, A.; Restagno, G.; Borghero, G.; Sabatelli, M.; Heckerman, D.; Rogaeva, E.; Zinman, L.; Rothstein, J. D.; Sendtner, M.; Drepper, C.; Eichler, E. E.; Alkan, C.; Abdullaev, Z.; Pack, S. D.; Dutra, A.; Pak, E.; Hardy, J.; Singleton, A.; Williams, N. M.; Heutink, P.; Pickering-Brown, S.; Morris, H. R.; Tienari, P. J.; Traynor, B. J.; The ITALSGEN Consortium. A hexanucleotide repeat expansion in C9ORF72 is the cause of chromosome 9p21-linked ALS-FTD. *Neuron* **2011**, *72*, 257−268.

(8) Cammas, A.; Millevoi, S. RNA G-quadruplexes: emerging mechanisms in disease. *Nucleic Acids Res.* **2017**, *45*, 1584−1595.

(9) Zhou, B.; Liu, C.; Geng, Y.; Zhu, G. Topology of a G-quadruplex DNA formed by C9orf72 hexanucleotide repeats associated with ALS and FTD. *Sci. Rep.* **2015**, *5*, No. 16673.
(10) Wang, E.; Thombre, R.; Shah, Y.; Latanich, R.; Wang, J. G-quadruplexes as pathogenic drivers in neurodegenerative disorders. *Nucleic Acids Res.* **2021**, *49*, 4816−4830.
(11) Wang, M.; Wang, W.; Kang, T. S.; Leung, C. H.; Ma, D. L. Development of an iridium(III) complex as a G-quadruplex probe and its application for the G-quadruplex-based luminescent detection of picomolar insulin. *Anal. Chem.* **2016**, *88*, 981−987.
(12) Liu, J. B.; Yang, C.; Ko, C. N.; Kasipandi, V.; Yang, B.; Lee, M. Y.; Leung, C. H.; Ma, D. L. A long lifetime iridium(III) complex as a sensitive luminescent probe for bisulfite detection in living zebrafish. *Sens. Actuators, B* **2017**, *243*, 971−976.
(13) Wang, W.; Yung, T. L.; Cheng, S. S.; Chen, F.; Liu, J. B.; Leung, C. H.; Ma, D. L. A long-lived luminogenic iridium(III) complex for acetylacetone detection in environmental samples. *Sens. Actuators, B* **2020**, *321*, No. 128486.
(14) Zamiri, B.; Reddy, K.; Macgregor, R. B., Jr.; Pearson, C. E. TMPyP4 porphyrin distorts RNA G-quadruplex structures of the disease-associated r(GGGGCC)n repeat of the C9orf72 gene and blocks interaction of RNA-binding proteins. *J. Biol. Chem.* **2014**, *289*, 4653−4659.
(15) Zhang, K.; Donnelly, C. J.; Haeusler, A. R.; Grima, J. C.; Machamer, J. B.; Steinwald, P.; Daley, E. L.; Miller, S. J.; Cunningham, K. M.; Vidensky, S.; Gupta, S.; Thomas, M. A.; Hong, I.; Chiu, S. L.; Huganir, R. L.; Ostrow, L. W.; Matunis, M. J.; Wang, J.; Sattler, R.; Lloyd, T. E.; Rothstein, J. D. The C9orf72 repeat expansion disrupts nucleocytoplasmic transport. *Nature* **2015**, *525*, 56−61.
(16) Su, Z.; Zhang, Y.; Gendron, T. F.; Bauer, P. O.; Chew, J.; Yang, W. Y.; Fostvedt, E.; Jansen-West, K.; Belzil, V. V.; Desaro, P.; Johnston, A.; Overstreet, K.; Oh, S. Y.; Todd, P. K.; Berry, J. D.; Cudkowicz, M. E.; Boeve, B. F.; Dickson, D.; Floeter, M. K.; Traynor, B. J.; Morelli, C.; Ratti, A.; Silani, V.; Rademakers, R.; Brown, R. H.; Rothstein, J. D.; Boylan, K. B.; Petrucelli, L.; Disney, M. D. Discovery of a biomarker and lead small molecules to target r(GGGGCC)-associated defects in c9FTD/ALS. *Neuron* **2014**, *83*, 1043−1050.
(17) Wang, Z. F.; Ursu, A.; Childs-Disney, J. L.; Guertler, R.; Yang, W. Y.; Bernat, V.; Rzuczek, S. G.; Fuerst, R.; Zhang, Y. J.; Gendron, T. F.; Yildirim, I.; Dwyer, B. G.; Rice, J. E.; Petrucelli, L.; Disney, M. D. The hairpin form of r(G4C2)(exp) in c9ALS/FTD is repeat-associated non-ATG translated and a target for bioactive small molecules. *Cell Chem. Biol.* **2019**, *26*, 179−190.
(18) Simone, R.; Balendra, R.; Moens, T. G.; Preza, E.; Wilson, K. M.; Heslegrave, A.; Woodling, N. S.; Niccoli, T.; Gilbert-Jaramillo, J.; Abdelkarim, S.; Clayton, E. L.; Clarke, M.; Konrad, M. T.; Nicoll, A. J.; Mitchell, J. S.; Calvo, A.; Chio, A.; Houlden, H.; Polke, J. M.; Ismail, M. A.; Stephens, C. E.; Vo, T.; Farahat, A. A.; Wilson, W. D.; Boykin, D. W.; Zetterberg, H.; Partridge, L.; Wray, S.; Parkinson, G.; Neidle, S.; Patani, R.; Fratta, P.; Isaacs, A. M. G-quadruplex-binding small molecules ameliorate C9orf72 FTD/ALS pathology in vitro and in vivo. *EMBO Mol. Med.* **2018**, *10*, 22−31.
(19) Zhang, Q.; An, Y.; Chen, Z. S.; Koon, A. C.; Lau, K. F.; Ngo, J. C. K.; Chan, H. Y. E. A Peptidylic Inhibitor for Neutralizing (r)(GGGGCC)(exp) -Associated Neurodegeneration in C9ALS-FTD. *Mol. Ther. Nucleic Acids* **2019**, *16*, 172−185.
(20) Mis, M. S. C.; Brajkovic, S.; Tafuri, F.; Bresolin, N.; Comi, G. P.; Corti, S. Development of therapeutics for C9ORF72 ALS/FTD-related disorders. *Mol. Neurobiol.* **2017**, *54*, 4466−4476.
(21) Martier, R.; Liefhebber, J. M.; Garcia-Osta, A.; Miniarikova, J.; Cuadrado-Tejedor, M.; Espelosin, M.; Ursua, S.; Petry, H.; van Deventer, S. J.; Evers, M. M.; Konstantinova, P. Targeting RNA-mediated toxicity in C9orf72 ALS and/or FTD by RNAi-based gene therapy. *Mol. Ther. Nucleic Acids* **2019**, *16*, 26−37.
(22) Yang, Q.; Jiao, B.; Shen, L. The development of C9orf72-related amyotrophic lateral sclerosis and frontotemporal dementia disorders. *Front. Genet.* **2020**, *11*, No. 562758.
(23) Balendra, R.; Isaacs, A. M. C9orf72-mediated ALS and FTD: multiple pathways to disease. *Nat. Rev. Neurol.* **2018**, *14*, 544−558.
(24) Kumar, V.; Hasan, G. M.; Hassan, M. I. Unraveling the role of RNA mediated toxicity of C9orf72 repeats in C9-FTD/ALS. *Front. Neurosci.* **2017**, *11*, No. 711.
(25) Haefner, B. Drugs from the deep: marine natural products as drug candidates. *Drug Discovery Today* **2003**, *8*, 536−544.
(26) Kumar, V.; Kashav, T.; Islam, A.; Ahmad, F.; Hassan, M. I. Structural insight into C9orf72 hexanucleotide repeat expansions: towards new therapeutic targets in FTD-ALS. *Neurochem. Int.* **2016**, *100*, 11−20.
(27) Zhou, B.; Geng, Y.; Liu, C.; Miao, H.; Ren, Y.; Xu, N.; Shi, X.; You, Y.; Lee, T.; Zhu, G. Characterizations of distinct parallel and antiparallel G-quadruplexes formed by two-repeat ALS and FTD related GGGGCC sequence. *Sci. Rep.* **2018**, *8*, No. 2366.
(28) Jansson, L. I.; Hentschel, J.; Parks, J. W.; Chang, T. R.; Lu, C.; Baral, R.; Bagshaw, C. R.; Stone, M. D. Telomere DNA G-quadruplex folding within actively extending human telomerase. *Proc. Natl. Acad. Sci. U.S.A.* **2019**, *116*, 9350−9359.
(29) Liu, C.; Zhou, B.; Geng, Y.; Tam, D. Y.; Feng, R.; Miao, H.; Xu, N.; Shi, X.; You, Y.; Hong, Y.; Tang, B. Z.; Lo, P. K.; Kuryavyi, V.; Zhu, G. A chair-type G-quadruplex structure formed by a human telomeric variant DNA in K(+) solution. *Chem. Sci.* **2019**, *10*, 218−226.
(30) Liu, C.; Geng, Y.; Miao, H.; Shi, X.; You, Y.; Xu, N.; Zhou, B.; Zhu, G. G-quadruplex structures formed by human telomeric DNA and C9orf72 hexanucleotide repeats. *Biophys. Rev.* **2019**, *11*, 389−393.
(31) Phan, A. T.; Kuryavyi, V.; Burge, S.; Neidle, S.; Patel, D. J. Structure of an unprecedented G-quadruplex scaffold in the human c-kit promoter. *J. Am. Chem. Soc.* **2007**, *129*, 4386−4392.
(32) Geng, Y. Y.; Liu, C. D.; Zhou, B.; Cai, Q. X.; Miao, H. T.; Shi, X.; Xu, N. N.; You, Y. Y.; Fung, C. P.; Din, R. U.; Zhu, G. The crystal structure of an antiparallel chair-type G-quadruplex formed by Bromo-substituted human telomeric DNA. *Nucleic Acids Res.* **2019**, *47*, 5395−5404.
(33) Mauger, D. M.; Lin, C.; Garcia-Blanco, M. A. Garcia-Blanco, hnRNP H and hnRNP F complex with Fox2 to silence fibroblast growth factor receptor 2 exon IIIc. *Mol. Cell. Biol.* **2008**, *28*, 5403−5419.
(34) Lee, Y. B.; Chen, H. J.; Peres, J. N.; Gomez-Deza, J.; Attig, J.; Stalekar, M.; Troakes, C.; Nishimura, A. L.; Scotter, E. L.; Vance, C.; Adachi, Y.; Sardone, V.; Miller, J. W.; Smith, B. N.; Gallo, J. M.; Ule, J.; Hirth, F.; Rogelj, B.; Houart, C.; Shaw, C. E. Hexanucleotide repeats in ALS/FTD form length-dependent RNA foci, sequester RNA binding proteins, and are neurotoxic. *Cell Rep.* **2013**, *5*, 1178−1186.
(35) Conlon, E. G.; Lu, L.; Sharma, A.; Yamazaki, T.; Tang, T.; Shneider, N. A.; Manley, J. L. The C9ORF72 GGGGCC expansion forms RNA G-quadruplex inclusions and sequesters hnRNP H to disrupt splicing in ALS brains. *eLife* **2016**, 5.
(36) Pang, W. L.; Hu, F. H. Cellular and physiological functions of C9ORF72 and implications for ALS/FTD. *J. Neurochem.* **2021**, *157*, 334−350.
(37) Brčić, J.; Plavec, J. Solution structure of a DNA quadruplex containing ALS and FTD related GGGGCC repeat stabilized by 8-bromodeoxyguanosine substitution. *Nucleic Acids Res.* **2015**, *43*, 8590−8600.
(38) Kondo, K.; Eguchi, T.; Kakinuma, K.; Mizoue, K.; Qiao, Y. F. Structure and biosynthesis of FD-594; a new antitumor antibiotic. *J. Antibiot.* **1998**, *51*, 288−295.
(39) Kang, H. S.; Brady, S. F. Arixanthomycins A-C: phylogeny-guided discovery of biologically active eDNA-derived pentangular polyphenols. *ACS Chem. Biol.* **2014**, *9*, 1267−1272.
(40) Kang, H. S.; Brady, S. F. Mining soil metagenomes to better understand the evolution of natural product structural diversity: pentangular polyphenols as a case study. *J. Am. Chem. Soc.* **2014**, *136*, 18111−18119.

https://doi.org/10.1021/acs.jmedchem.2c00654
J. Med. Chem. 2022, 65, 12825−12837

(41) Wang, P.; Zhang, W. J.; Zhan, J. X.; Tang, Y. Identification of oxyE as an ancillary oxygenase during tetracycline biosynthesis. *ChemBioChem* **2009**, *10*, 1544−1550.
(42) Gao, C. Z.; Guo, Z. Y.; Lu, X. Z.; Chen, H. Y.; Liu, L. W.; Yu, Z. G.; Chen, Y. H. Hexaricins, pradimicin-like polyketides from a marine sediment-derived streptosporangium sp and their antioxidant effects. *J. Nat. Prod.* **2018**, *81*, 2069−2074.
(43) Morris, G. M.; Goodsell, D. S.; Halliday, R. S.; Huey, R.; Hart, W. E.; Belew, R. K.; Olson, A. J. Automated docking using a lamarckian genetic algorithm and an empirical binding free energy function. *J. Comput. Chem.* **1998**, *19*, 1639−1662.
(44) Morris, G. M.; Huey, R.; Lindstrom, W.; Sanner, M. F.; Belew, R. K.; Goodsell, D. S.; Olson, A. J. AutoDock4 and AutoDockTools4: automated docking with selective receptor flexibility. *J. Comput. Chem.* **2009**, *30*, 2785−2791.

https://doi.org/10.1021/acs.jmedchem.2c00654
J. Med. Chem. 2022, 65, 12825−12837